2018 European Control Conference (ECC)
June 12-15, 2018. Limassol, Cyprus

A Simple Optimal Planer Path Following Algorithm for Unmanned Aerial Vehicles*

Jun Yang[1,2], Cunjia Liu[2], Zongyu Zuo[3] and Wen-Hua Chen[2]

Abstract— **In this paper, we present a simple optimal path following algorithm for a generic small fixed-wing unmanned aerial vehicle by virtue of a predictive control approach. Different from most of exiting path following algorithms, the proposed algorithm is designed in an optimal manner where the control action is generated based on a well-defined cost function. In addition, the presented approach is designed without resorting to any complex geometric coordinate transformation. Thereby the resultant optimal control law is straightforward for practical implementation. The effectiveness of the present method is validated by three cases of simulation studies.**

I. INTRODUCTION

One of the most common task of unmanned aerial vehicles (UAVs) is to cruise along a predefined geometric path [1]–[3]. For these applications, the UAVs should travel on the path, while it is not necessary to force the UAVs to a certain time parameterized point. For the purpose of minimizing fuel consumption, the fixed-wing UAVs are generally designed to fly with a given constant airspeed [4]. In the context of trajectory tracking, the heading angle of the vehicle has to be adjusted to regulate the two planar tracking errors in the inertial frame. This will result in a typical underactuated control problem given constant airspeed. Consequently, by designing additional dynamics of the decision parameter in the given geometric path, the path following control approach has been presented to address this problem [5]–[7].

Due to the practicality and significance, the path following control problem has been extensively investigated in various literatures. In general, the path following problem is solved via the following two steps. First, geometric based methods, such as virtual target point (VTP) approach [8] and vector field approach [9] can be used. In terms of VTP approaches, the Serret-Frenet frame transformation is usually employed, the path following problem is then transferred to the tracking control problem, where the tracking errors are defined as the position errors between the UAV and the VTP. Second, advanced control approaches are employed to address several challenging issues involved in the above well-formulated tracking control problems. For examples, a nested saturation control approach is presented in [4] to solve the input constraints problem of fixed-wing UAV path following. A disturbance rejection control approach is utilized in [10] to improve the robustness of the path following algorithm against external wind gusts.

In spite of extensive results on the path following problems, they generally exhibit two drawbacks. Firstly, the utilized geometric methods usually bring complex frame transformation and result in involved control algorithms for implementation. Second, the evolutionary law of the geometric path parameter of the predefined path is designed separately from the roll angle design of the UAVs. As such, the path parameter law is not produced in an optimized way that ensuring overall optimized path following performance. In a recent work [11], a nonlinear model predictive control approach is proposed for constrained output path following of a class of affine nonlinear systems. A novel idea therein is that the design of parameter law of the path is integrated within the cost function for optimization.

Motivated by [11], we present a new and simpler optimal path following algorithm for a small-scale fixed-wing UAV. However, different from [11], the present paper utilizes an explicit nonlinear predictive control design approach for the path following problem of UAVs. The proposed controller provides an explicit form solution without any online optimization computation that gives an intuitive way for implementation. In addition, the path following errors are regulated in an optimal manner which ensures better path following performance in the sense that both the roll angle and the evolvement of the path parameter are manipulated as decision variables for the optimal path following. Detailed guidelines for control order and prediction horizon selection that guaranteeing asmptotical stability has also been discussed in this paper. Simulation scenarios on circle orbit path following are carried out to validate the presented optimal path following algorithm. The results show that the proposed path following algorithm exhibits promising following performances.

II. PROBLEM FORMULATION

This paper aims to propose an optimal path following control algorithm for a generic fixed-wing UAVs. The UAVs are supposed to cruise at a constant speed for the purpose of saving energy [4]. The planar motion of a generic small-scale

*This work was supported in part by the UK Engineering and Physical Science Research Council (EPSRC) under the Grant EP/P012868/1, and in part by National Natural Science Foundation of China (NSFC) under the Grants 61573099 and 61633003.

[1]J. Yang is with School of Automation, Southeast University, Nanjing 210096, China, and he is also with the Department of Aeronautical and Automative Engineering, Loughborough University, LE11 3TU, UK junyang8402@gmail.com

[2]C. Liu and W.-H. Chen are with the Department of Aeronautical and Automative Engineering, Loughborough University, LE11 3TU, UK {c.liu5,w.chen}@lboro.ac.uk

[3]Z. Zuo is with the Seventh Research Division, Beihang University, Beijing 100191, China zzybobby@buaa.edu.cn

fixed-wing UAVs is described as

$$\begin{aligned}\dot{x} =& V\cos\psi\\ \dot{y} =& V\sin\psi\\ \dot{\psi} =& \frac{g}{V}\tan\phi_c\end{aligned} \tag{1}$$

where x and y denote the positions of the UAV on the plane, V represents the velocity of the UAV, ψ is the heading angle, and ϕ_c is the command of roll angle that serving as the control input.

The desired geometric path of the UAV in the output space is given by

$$\mathcal{P} = \left\{x, y \in \mathbb{R} | \theta \in [\underline{\theta}, \overline{\theta}] \mapsto x = p_1(\theta), y = p_2(\theta)\right\} \tag{2}$$

where θ is the path parameter, $\underline{\theta}$ and $\overline{\theta}$ denote the minimum and maximum values of the path parameter. The path following problem is thereby transferred to the following tracking control problem

$$\begin{aligned}\dot{x} =& V\cos\psi\\ \dot{y} =& V\sin\psi\\ \dot{\psi} =& \frac{g}{V}\tan\phi_c\\ \dot{\theta}_1 =& \theta_2\\ \dot{\theta}_2 =& \mu\\ e_1 =& x - p_1(\theta)\\ e_2 =& y - p_2(\theta)\\ \theta_1 =& \theta,\ \theta_2 = \dot{\theta}\end{aligned} \tag{3}$$

where μ is the virtual control law that will generate the path reference to be followed. Note that the present path following algorithm admits an additional design freedom of airspeed. That means regulation of airspeed is not required to realize path following here. The varying airspeed as per practical desire is acceptable for the proposed path following algorithm. The objective of this paper is to design an optimal control law such that output path following errors converge to zero asymptotically by means of optimization, that is, $x(t) \to p_1(\theta(t))$ and $y(t) \to p_2(\theta(t))$ as $t \to \infty$.

III. OPTIMAL OUT PATH FOLLOWING

For the sake of convenience, we will use $\omega = \frac{g}{V}\tan\phi_c$ in the following derivations. Let $\mathrm{x} = [x, y, \psi, \theta_1, \theta_2]^T \in \mathbb{R}^5$, $\mathrm{u} = [\omega, \mu]^T \in \mathbb{R}^2$ and $\mathrm{e} = [e_1, e_2]^T \in \mathbb{R}^2$. The dynamics of system (3) is described in the following compact form

$$\begin{aligned}\dot{\mathrm{x}} =& \mathrm{f(x)} + \mathrm{Gu}\\ \mathrm{e} =& \mathrm{h(x)}\end{aligned} \tag{4}$$

where

$$\mathrm{f(x)} = \begin{bmatrix} V\cos\psi \\ V\sin\psi \\ 0 \\ \theta_2 \\ 0 \end{bmatrix}, \mathrm{G} = \begin{bmatrix} 0 & 0 \\ 0 & 0 \\ 1 & 0 \\ 0 & 0 \\ 0 & 1 \end{bmatrix},$$

$$\mathrm{h(x)} = \begin{bmatrix} x - p_1(\theta) \\ y - p_2(\theta) \end{bmatrix}$$

A. Path Tracking Error Prediction

To begin with, the cost function of the output path following problem for the UAV (1) is defined as

$$J = \frac{1}{2}\int_0^{T_P} \bar{\mathrm{e}}^T(t+\tau) Q \bar{\mathrm{e}}(t+\tau) d\tau, \tag{5}$$

where T_P is the predictive period, Q is the error weighting matrix that is symmetric and positive definite, and $\bar{\mathrm{e}}(t) = [\bar{e}_1(t), \bar{e}_2(t)]^T$ is the predicted output path following error vector. The future output path following error $\bar{e}_i(t+\tau)$ in the moving horizon is predicted by Taylor series expansion

$$\bar{e}_i(t+\tau) = e_i(t) + \tau e_i^{(1)}(t) + \cdots + \frac{\tau^{2+r}}{(2+r)!} e_i^{(2+r)}(t), \tag{6}$$

where r is the control order [12]. The time derivatives of $e_i(t)$ are calculated and represented as

$$\dot{e}_i = L_{\mathrm{f}} h_i(\mathrm{x}), \tag{7}$$

where $L_{\mathrm{f}} h_i(\mathrm{x}) := \frac{\partial h_i(\mathrm{x})}{\partial \mathrm{x}} \mathrm{f(x)}$ is the standard Lie derivatives [13]. Differentiating Eq. (7) with respect to time yields

$$\ddot{e}_i = L_{\mathrm{f}}^2 h_i(\mathrm{x}) + L_{\mathrm{G}} L_{\mathrm{f}} h_i(\mathrm{x}) \mathrm{u}, \tag{8}$$

Continuously taking derivative of (8) gives

$$e_i^{(3)} = L_{\mathrm{f}}^3 h_i(\mathrm{x}) + L_{\mathrm{G}} L_{\mathrm{f}} h_i(\mathrm{x}) \dot{\mathrm{u}} + p_i^1(\mathrm{x}, \mathrm{u}), \tag{9}$$

where

$$p_i^1(\mathrm{x}, \mathrm{u}) = L_{\mathrm{G}} L_{\mathrm{f}} h_i(\mathrm{x}) \mathrm{u} + \frac{d L_{\mathrm{G}} L_{\mathrm{f}} h_i(\mathrm{x})}{dt} \mathrm{u}. \tag{10}$$

Similarly, the higher derivatives of $e_i(t)$ can be calculated as

$$\begin{aligned} e_i^{(2+k)} =& L_{\mathrm{f}}^{2+k} h_i(\mathrm{x}) + L_{\mathrm{G}} L_{\mathrm{f}} h_i(\mathrm{x}) \mathrm{u}^{(k)} \\ &+ p_i^k(\mathrm{x}, \mathrm{u}, \ldots, \mathrm{u}^{(k-1)}), \end{aligned} \tag{11}$$

for $k = 2, \ldots, r$.

The predictive output path following error $\bar{\mathrm{e}}(t+\tau)$ is defined as

$$\bar{\mathrm{e}}(t+\tau) = \begin{bmatrix} \bar{e}_1(t+\tau) \\ \bar{e}_2(t+\tau) \end{bmatrix} = \begin{bmatrix} \bar{\mathcal{T}}, & \tilde{\mathcal{T}} \end{bmatrix} \begin{bmatrix} \bar{Y} \\ \tilde{Y} \end{bmatrix}, \tag{12}$$

where

$$\bar{\mathcal{T}} = \begin{bmatrix} 1 & \tau & 0 & 0 \\ 0 & 0 & 1 & \tau \end{bmatrix},$$

$$\tilde{\mathcal{T}} = \begin{bmatrix} \tilde{\tau}_1 & \cdots & \tilde{\tau}_{r+1} \end{bmatrix},$$

$$\tilde{Y} = \begin{bmatrix} \tilde{Y}_1 \\ \vdots \\ \tilde{Y}_{r+1} \end{bmatrix}, \bar{Y} = \begin{bmatrix} e_1 \\ \dot{e}_1 \\ e_2 \\ \dot{e}_2 \end{bmatrix},$$

with

$$\tilde{\tau}_i = \mathrm{diag}\left\{\frac{\tau^{i+1}}{(i+1)!}, \frac{\tau^{i+1}}{(i+1)!}\right\},$$

and

$$\tilde{Y}_i = \left[e_1^{(i+1)}, \ e_2^{(i+1)}\right]^T,$$

for $i = 1, \ \ldots \ , r+1$.

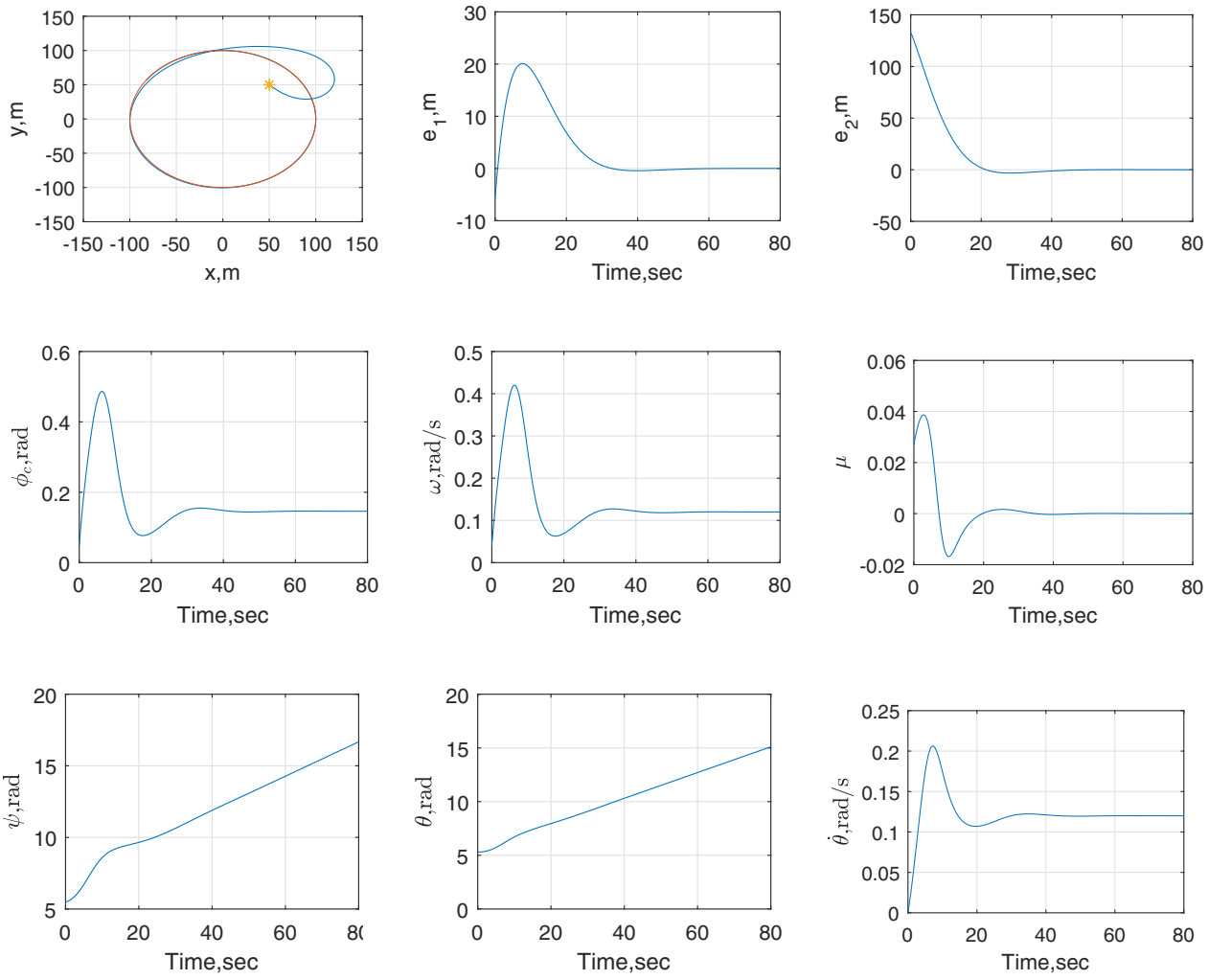

Fig. 1. (top left) Desired path and actual path (the star denotes the starting point); (top middle) East direction path following error e_1; (top right) North direction path following error e_2; (middle left) roll angle command ϕ_c; (central) roll rate ω; (middle right) the virtual control μ; (bottom left) the heading angle ψ; (bottom middle) the path parameter θ; and (bottom right) the path virtual state $\dot{\theta}$. (*Case I*).

B. Receding Horizon Optimization

Note that $\bar{Y}$ and $\tilde{Y}$ are regardless of τ. The performance index (5) is then rewritten as

$$\begin{aligned} J =& \frac{1}{2}\int_0^{T_P} \left[\bar{Y}^T, \tilde{Y}^T\right] \begin{bmatrix} \bar{\mathcal{T}}^T \\ \tilde{\mathcal{T}}^T \end{bmatrix} Q \left[\bar{\mathcal{T}},\ \tilde{\mathcal{T}}\right] \begin{bmatrix} \bar{Y} \\ \tilde{Y} \end{bmatrix} d\tau \\ =& \left[\bar{Y}^T, \tilde{Y}^T\right] \begin{bmatrix} \mathcal{T}_1 & \mathcal{T}_2 \\ \mathcal{T}_2^T & \mathcal{T}_3 \end{bmatrix} \begin{bmatrix} \bar{Y} \\ \tilde{Y} \end{bmatrix}, \end{aligned} \tag{13}$$

where

$$\mathcal{T}_1 = \int_0^{T_P} \bar{\mathcal{T}}^T Q \bar{\mathcal{T}} d\tau,$$

$$\mathcal{T}_2 = \int_0^{T_P} \bar{\mathcal{T}}^T Q \tilde{\mathcal{T}} d\tau,$$

$$\mathcal{T}_3 = \int_0^{T_P} \tilde{\mathcal{T}}^T Q \tilde{\mathcal{T}} d\tau.$$

Let $\bar{\mathrm{u}} = \left[\mathrm{u}^T,\ \dot{\mathrm{u}}^T, \ldots,\ \left(\mathrm{u}^{(r)}\right)^T\right]$. Then one obtains

$$\frac{\partial J}{\partial \bar{\mathrm{u}}} = \left(\frac{\partial \tilde{Y}}{\partial \bar{\mathrm{u}}}\right)^T \mathcal{T}_2^T \bar{Y} + \left(\frac{\partial \tilde{Y}}{\partial \bar{\mathrm{u}}}\right)^T \mathcal{T}_3 \tilde{Y} = 0. \tag{14}$$

It can be verified that $\partial \tilde{Y}/\partial \bar{\mathrm{u}}$ is nonsingular, which implies that

$$\tilde{Y} = -\mathcal{T}_3^{-1} \mathcal{T}_2^T \bar{Y}. \tag{15}$$

The first two rows of Eq. (15) are written as

$$\tilde{Y}_1 = -K\bar{Y}, \tag{16}$$

where K is the first two rows of the matrix $\mathcal{T}_3^{-1}\mathcal{T}_2^T$. The nonlinear MPC law is solved from (16), given by

$$\mathrm{u}^*(t) = A^{-1}(\mathrm{x}) \left[-K\bar{Y} - B(\mathrm{x})\right], \tag{17}$$

where

$$A(\mathrm{x}) = \begin{bmatrix} L_\mathrm{G} L_\mathrm{f} h_1 \\ L_\mathrm{G} L_\mathrm{f} h_2 \end{bmatrix},$$

$$B(\mathrm{x}) = \begin{bmatrix} L_{\mathrm{f}}^2 h_1 \\ L_{\mathrm{f}}^2 h_2 \end{bmatrix},$$

$$\bar{Y} = [h_1, L_{\mathrm{f}} h_1, h_2, L_{\mathrm{f}} h_2]^T.$$

It follows from that the optimized control gain K has the following form

$$K = \begin{bmatrix} k_{10} & k_{11} & 0 & 0 \\ 0 & 0 & k_{20} & k_{21} \end{bmatrix}.$$

The parameters k_{ij} $(i = 1, 2; j = 0, 1)$ are determined by the predictive period T_P and control order r.

C. Stability Analysis

Collecting the error dynamics of each output path tracking error given in (8), the full dimensional error dynamics are given by

$$\begin{bmatrix} \ddot{e}_1 \\ \ddot{e}_2 \end{bmatrix} = \begin{bmatrix} L_{\mathrm{f}}^2 h_1 \\ L_{\mathrm{f}}^2 h_2 \end{bmatrix} + \begin{bmatrix} L_{\mathrm{G}} L_{\mathrm{f}} h_1 \\ L_{\mathrm{G}} L_{\mathrm{f}} h_2 \end{bmatrix} \mathrm{u}. \tag{18}$$

Substituting the optimal control law (17) into (18), the dynamic closed-loop system is then governed by

$$\ddot{\bar{\mathrm{e}}} = -K\bar{Y}. \tag{19}$$

With the structure of K and the definition of $\bar{Y}$ in mind, the closed-loop system (19) is rewritten as

$$\begin{aligned} \ddot{e}_1 + k_{11}\dot{e}_1 + k_{10} e_1 &= 0 \\ \ddot{e}_2 + k_{21}\dot{e}_2 + k_{20} e_2 &= 0 \end{aligned} \tag{20}$$

Clearly, the closed-loop system is exponentially stable as long as $k_{ij} > 0$ $(i = 1, 2; j = 0, 1)$. Note that all the elements in matrices $\mathcal{T}_2$ and $\mathcal{T}_3$ are positive for arbitrary control order r and predictive period T_P. This implies that $k_{ij} > 0$ $(i = 1, 2; j = 0, 1)$ for any control order and predictive period. Consequently, the exponential stability of the closed-loop system is guaranteed for any control order and predictive period.

IV. CASE STUDIES-ORBIT PATH FOLLOWING

A. Orbit Path Following Algorithm

Without lose of generality, the orbit path to be followed is depicted by

$$p_1(\theta) = 100\cos\theta, p_2(\theta) = 100\sin\theta.$$

We thus have

$$\frac{\partial p_1}{\partial \theta} = -100\sin\theta, \frac{\partial p_2}{\partial \theta} = 100\cos\theta,$$

$$\frac{\partial^2 p_1}{\partial \theta^2} = -100\cos\theta, \frac{\partial^2 p_2}{\partial \theta^2} = -100\sin\theta.$$

With various intuitive calculations, one obtains

$$A(\mathrm{x}) = \begin{bmatrix} -V\sin\psi & 100\sin\theta \\ V\cos\psi & -100\cos\theta \end{bmatrix},$$

$$B(\mathrm{x}) = \begin{bmatrix} 100\theta_2^2\cos\theta \\ 100\theta_2^2\sin\theta \end{bmatrix},$$

$$\bar{Y} = [h_1, L_{\mathrm{f}} h_1, h_2, L_{\mathrm{f}} h_2]^T,$$

with

$$h_1 = x - 100\cos\theta, L_{\mathrm{f}} h_1 = V\cos\psi + 100\theta_2\sin\theta$$

$$h_2 = y - 100\sin\theta, L_{\mathrm{f}} h_2 = V\sin\psi - 100\theta_2\cos\theta$$

Define the following virtual control input as

$$\nu_1 = -k_{10}h_1 - k_{11}L_{\mathrm{f}}h_1 - L_{\mathrm{f}}^2 h_1$$

$$\nu_2 = -k_{20}h_2 - k_{21}L_{\mathrm{f}}h_2 - L_{\mathrm{f}}^2 h_2$$

With the above denotations, the optimal control inputs (17) solving the orbit path following are given by

$$\begin{bmatrix} \omega \\ \mu \end{bmatrix} = \csc(\theta - \psi) \begin{bmatrix} \frac{\cos\theta}{V} & \frac{\sin\theta}{V} \\ \frac{\cos\psi}{100} & \frac{\sin\psi}{100} \end{bmatrix} \begin{bmatrix} \nu_1 \\ \nu_2 \end{bmatrix} \tag{21}$$

or

$$\begin{bmatrix} \omega \\ \mu \end{bmatrix} = \begin{bmatrix} (\nu_1\cos\theta + \nu_2\sin\theta)\csc(\theta - \psi)/V \\ (\nu_1\cos\psi + \nu_2\sin\psi)\csc(\theta - \psi)/100 \end{bmatrix} \tag{22}$$

B. Simulation Results

Suppose that the desired path following direction is anti-clockwise. To make the simulation scenarios more challenging, we consider the initial heading angle of the UAV with the direction opposite to the direction of the circular path. Without lose of generality, the airspeed of the UAV is considered as a constant of $V = 15$ m/s and we set $\psi(0) = 7\pi/4$ rad. The initial states representing the path curves are selected as $\theta(0) = 27\pi/16$ rad, $\dot{\theta}(0) = 0$ rad/s. The predictive period and control order of the predictive controller are designed as $T_P = 25$ and $r = 1$, respectively. The weighting matrix Q is assigned as an identity matrix. We consider three cases of simulation scenarios in this paper. The first one is concerned with the case that the initial UAV position is inside the circular path, while the second accounts for the case the initial UAV position located outside the circular path. The last case takes into account the external disturbances to test the robustness of the path following algorithm.

1) Case I-The Initial UAV Position Inside The Orbit: In this case, the initial UAV position $x(0) = 50$ m and $y(0) = 50$ m is taken into account in this part. The response curves of output path following in the this case are shown in Fig. 1.

It can be observed from Fig. 1 that the UAV is initially inside the orbit circle path, and the initial heading angle is pointing to the clockwise direction that is opposite to the desired path direction. This brings challenges for the path following problem as the heading angle should be adjusted significantly in the initial stage such that the UAV could follow the desired geometric path in anti-clockwise direction. As shown by Fig. 1(a), the proposed optimal path following control algorithm admits a fine path following profile. It is observed from Fig. 1(b) and (c) that the output path following errors converge to zero smoothly without any steady-state errors. The profiles of the roll rate, the heading angle as well as other virtual states and control input are also smooth as shown by Fig. 1(d)-(h).

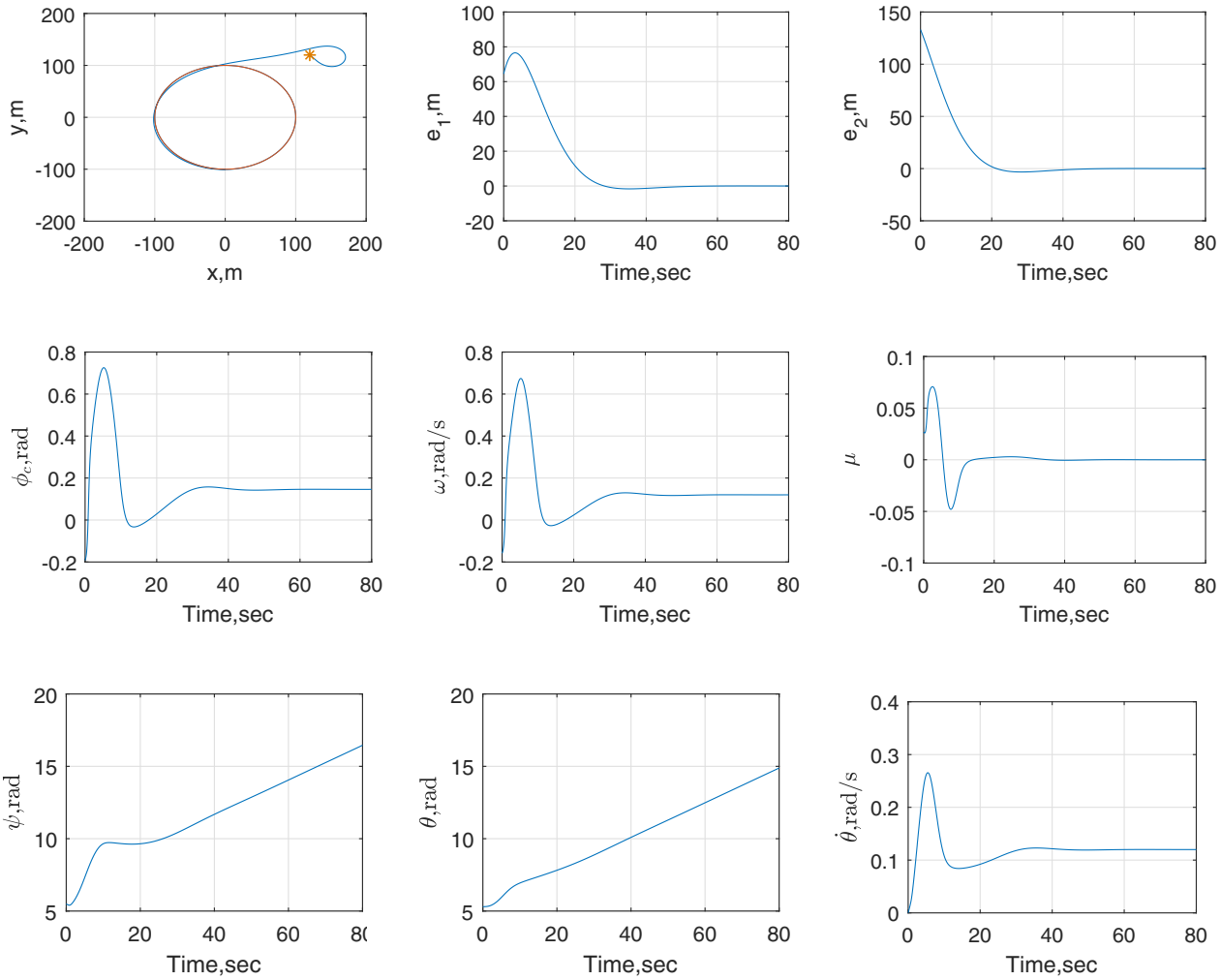

Fig. 2. (top left) Desired path and actual path (the star denotes the starting point); (top middle) East direction path following error e_1; (top right) North direction path following error e_2; (middle left) roll angle command ϕ_c; (central) roll rate ω; (middle right) the virtual control μ; (bottom left) the heading angle ψ; (bottom middle) the path parameter θ; and (bottom right) the path virtual state $\dot{\theta}$. (*Case II*).

2) Case II-The Initial UAV Position Outside The Orbit: In contrary to Case I, we consider that the initial UAV position is given by $x(0) = 120$ m and $y(0) = 120$ m, which is located outside the circle of the desired path. The resultant response curves of the closed-loop system are shown in Fig. 2. In such a different case, we can derive similar path following control performance as that of *Case I*.

3) Case III-The External Wind Disturbance Case: In this case, the initial UAV position $x(0) = 50$ m and $y(0) = 50$ m is still used. The external wind disturbances in x and y directions are both taken as $2\sin(0.1t)$ m/s. The response curves of output path following in the this case are shown in Fig. 3. As shown by Fig. 3, the proposed path following algorithm could guarantee bounded following errors. However, there are still considerable offsets for the proposed algorithm. It deserves further studies to investigate the robustness performance of the proposed path following algorithm in the presence of external wind disturbances.

V. Conclusion

In this paper, an optimal path following control algorithm has been presented for a generic fixed-wing UAVs without resorting to any geometric transformations. It has been shown that the closed-loop system is exponentially stable for arbitrary feasible control order and predictive period. A major merit of the presented approach lies in that it is suitable for more general geometric path following rather than limited curvature like straight line and circular orbit. Finally, a circular orbit path following case study has been carried out to validate the feasibility and effectiveness.

References

[1] A. P. Aguiar, J. P. Hespanha, and P. V. Kokotović, Performance limitations in reference tracking and path following for nonlinear systems, Automatica, vol. 44, no. 3, pp. 598-610, 2008.

[2] G. Ambrosino, M. Ariola, U. Ciniglio, F. Corraro, E. De Lellis, and A. Pironti, Path generation and tracking in 3-D for UAVs, IEEE Transactions on Control Systems Technology, vol. 17, no. 4, pp. 980-988, 2009.

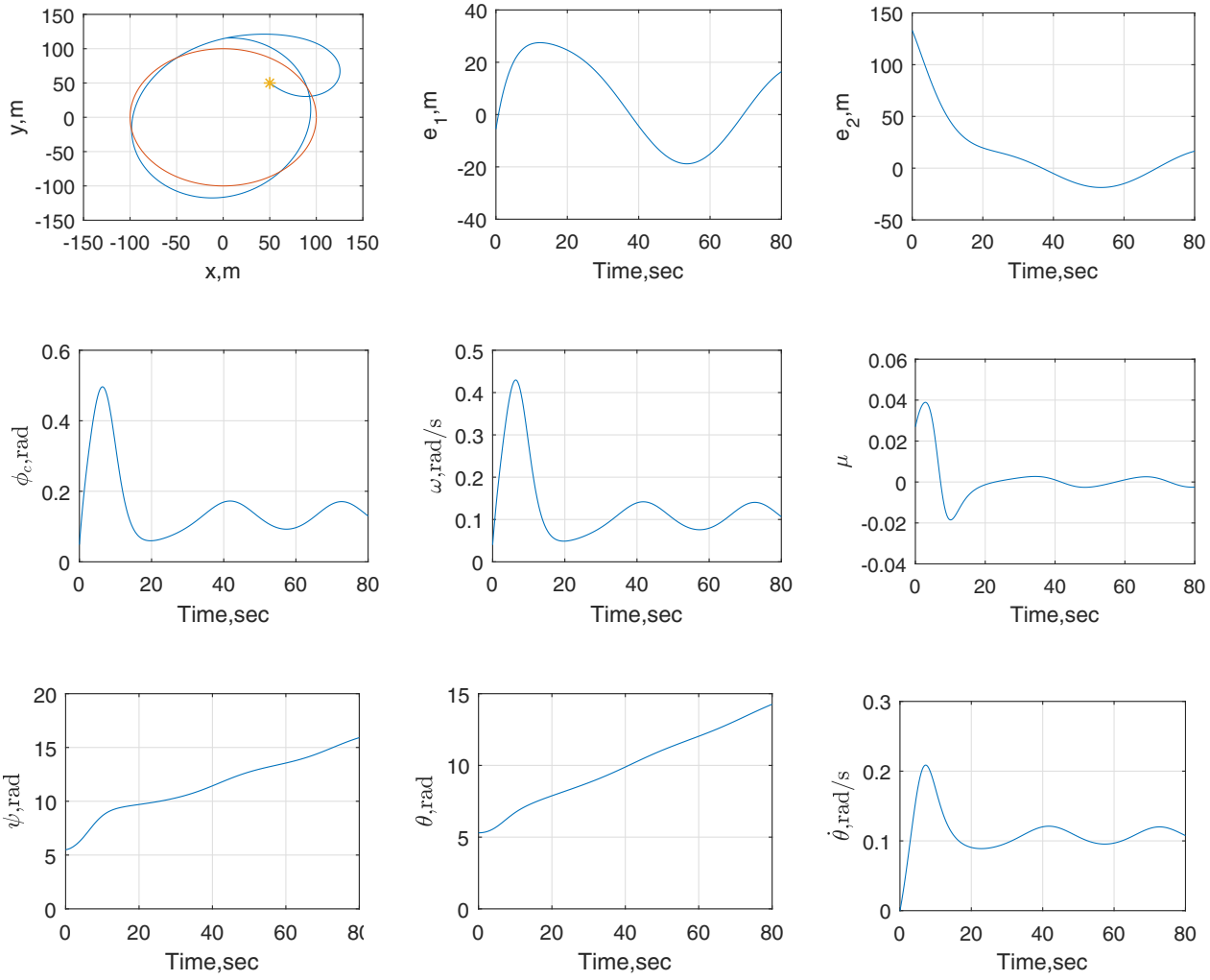

Fig. 3. (top left) Desired path and actual path (the star denotes the starting point); (top middle) East direction path following error e_1; (top right) North direction path following error e_2; (middle left) roll angle command ϕ_c; (central) roll rate ω; (middle right) the virtual control μ; (bottom left) the heading angle ψ; (bottom middle) the path parameter θ; and (bottom right) the path virtual state $\dot{\theta}$. (*Case III*).

[3] P. B. Sujit, S. Saripalli, and J. B. Sousa, Unmanned aerial vehicle path following: A survey and analysis of algorithms for fixed-wing unmanned aerial vehicless. IEEE Control Systems Magzine, vol. 34, no. 1, pp. 42-59, 2014.

[4] R. W. Beard, J. Ferrin, and J. Humpherys, Fixed wing UAV path following in wind with input constraints, IEEE Transactions on Control Systems Technology, vol. 22, no. 6, pp. 2103-2117.

[5] N. Cho, Y. Kim, and S. Park, Three-dimensional nonlinear differential geometric path-following guidance law, Journal of Guidance Control and Dynamics, vol. 38, no. 12, pp. 2366-2385, 2015.

[6] R. Rysdyk, Unmanned aerial vehicle path following for target observation in wind, Journal of Guidance Control and Dynamics, vol. 29, no. 5, pp. 1092-1100, 2006.

[7] S. Lee, A. Cho, and C. Kee, Integrated waypoint path generation and following of an unmanned aerial vehicle, Aircraft Engineering and Aerospace Technology, vol. 82, no. 5, pp. 296-304, 2010.

[8] A. P. Aguiar, and J. P. Hespanha, Trajectory-tracking and path-following of underactuated autonomous vehicles with parametric modeling uncertainty, IEEE Transactions on Automatic Control, vol. 52, no. 8, pp. 1362-1379, 2007.

[9] D. R. Nelson, D. B. Barber, T. W. McLain, and R. W. Beard, Vector field path following for miniature air vehicles, IEEE Transactions on Robotics, vol. 23, no. 3, pp. 519-529, 2007.

[10] C. Liu, O. McAree, and W.-H. Chen, Path-following control for small fixed-wing unmanned aerial vehicles under wind disturbances, International Journal of Robust and Nonlinear Control, vol. 23, no. 15, pp. 1682-1698, 2013.

[11] T. Faulwasser and R. Findeisen, Nonlinear model predictive control for constrained output path following, IEEE Transactions on Automatic Control, vol. 61, no. 4, pp. 1026-1039, 2016.

[12] W.-H. Chen, D. J. Ballance, and P. J. Gawthrop, Optimal control of nonlinear systems: a predictive control approach, Automatica, vol. 39, no. 4, pp. 633-641, 2003.

[13] A. Isidori, *Nonlinear Control Systems*, London: Springer, 2013.